

Pole determination of $P_{\psi_s}^\Lambda(4338)$ and possible $P_{\psi_s}^\Lambda(4254)$ in $B^- \rightarrow J/\psi\Lambda\bar{p}$

S.X. Nakamura^{1,2,*} and J.-J. Wu^{3,†}

¹University of Science and Technology of China, Hefei 230026, People's Republic of China

²State Key Laboratory of Particle Detection and Electronics (IHEP-USTC), Hefei 230036, People's Republic of China

³School of Physical Sciences, University of Chinese Academy of Sciences (UCAS), Beijing 100049, China

First hidden-charm pentaquark candidate with strangeness, $P_{\psi_s}^\Lambda(4338)$, was recently discovered in $B^- \rightarrow J/\psi\Lambda\bar{p}$ by the LHCb Collaboration. $P_{\psi_s}^\Lambda(4338)$ shows up as a bump at the $\Xi_c\bar{D}$ threshold in the $J/\psi\Lambda$ invariant mass ($M_{J/\psi\Lambda}$) distribution. The $M_{J/\psi\Lambda}$ distribution also shows a large fluctuation at the $\Lambda_c\bar{D}_s$ threshold, hinting the existence of a possible $P_{\psi_s}^\Lambda(4254)$. In this work, we determine the $P_{\psi_s}^\Lambda(4338)$ and $P_{\psi_s}^\Lambda(4254)$ pole positions for the first time. For this purpose, we fit a $B^- \rightarrow J/\psi\Lambda\bar{p}$ model to the $M_{J/\psi\Lambda}$, $M_{J/\psi\bar{p}}$, $M_{\Lambda\bar{p}}$, and $\cos\theta_{K^*}$ distributions from the LHCb simultaneously; $\chi^2/\text{ndf} \sim 1.29$. Then we extract $P_{\psi_s}^\Lambda$ poles from a unitary $\Xi_c\bar{D}$ - $\Lambda_c\bar{D}_s$ coupled-channel scattering amplitude built in the model. The $P_{\psi_s}^\Lambda(4338)$ pole is found at $(4339.2 \pm 2.7) - (0.9 \pm 0.1)i$ MeV while the $P_{\psi_s}^\Lambda(4254)$ pole at 4254.4 ± 0.8 MeV. Without the coupled-channels, $P_{\psi_s}^\Lambda(4338)$ is a bound $\Xi_c^+ D^-$ -virtual $\Xi_0^+ \bar{D}^0$ state while $P_{\psi_s}^\Lambda(4254)$ is a $\Lambda_c\bar{D}_s$ virtual state. The data disfavors a hypothesis of $P_{\psi_s}^\Lambda(4338)$ as merely a kinematical effect. This pole determination, which is important in its own right, sets a primary basis to study the nature of the $P_{\psi_s}^\Lambda$ states.

Introduction.— Since the foundation of the quark model, we have been addressing the fundamental question: “What form of the matter can be built from quarks?” Recent experimental discoveries of pentaquark and tetraquark candidates have decisively widened our territory of the conventional qqq and $q\bar{q}$ hadrons to include qualitatively different $qqqq\bar{q}$, $qq\bar{q}\bar{q}$, and even more exotic structures; see reviews [1–8]. Establishing the (non-)existence of pentaquark and tetraquark states is now essential to answer the above fundamental question.

The existence of hidden-charm pentaquarks with strangeness ($P_{\psi_s}^\Lambda$, $udsc\bar{c}$) has been expected theoretically [9–11], and the discovery of hidden-charm pentaquark candidates ($uudc\bar{c}$) [12, 13] further strengthened the expectation [14–19]. The first evidence (3.1σ) of $P_{\psi_s}^\Lambda$ was found, by the LHCb Collaboration, in $\Xi_b^- \rightarrow J/\psi\Lambda K^-$ as a bump at ~ 4459 MeV in the $J/\psi\Lambda$ invariant mass ($M_{J/\psi\Lambda}$) distribution [20]. This result invited lots of theoretical studies on $P_{\psi_s}^\Lambda(4459)$ [21–35]. Then, very recently, the LHCb announced the first discovery ($> 10\sigma$) of $P_{\psi_s}^\Lambda$ in $B^- \rightarrow J/\psi\Lambda\bar{p}$ [36]. Their amplitude analysis determined the mass and width of $P_{\psi_s}^\Lambda$ to be

$$4338.2 \pm 0.7 \text{ MeV}, \quad 7.0 \pm 1.2 \text{ MeV}, \quad (1)$$

respectively, and the spin-parity (J^P) to be $1/2^-$. In response to the discovery, proposals have been made to interpret $P_{\psi_s}^\Lambda(4338)$ as a $\Xi_c\bar{D}$ molecule [37–39], and also as a triangle singularity [40].

To understand the nature of $P_{\psi_s}^\Lambda(4338)$, its properties such as the mass, width, and J^P are the crucial information. The LHCb amplitude analysis obtained these information in Eq. (1), under an assumption that the $P_{\psi_s}^\Lambda(4338)$ peak is due to a resonance that can be well simulated by a Breit-Wigner (BW) amplitude. However, the $P_{\psi_s}^\Lambda(4338)$ peak is located right on the $\Xi_c\bar{D}$ threshold [see Fig. 2(a)], which would invalidate this assumption.

First of all, the resonancelike structure might be caused by a kinematical effect (threshold cusp) and not by a resonance pole [41]. If a $P_{\psi_s}^\Lambda(4338)$ pole exists and it couples with the $\Xi_c\bar{D}$ channel, the BW amplitude is still not suitable since it does not account for: (i) the width starts to increase rapidly as the $\Xi_c\bar{D}$ channel opens; (ii) the lineshape due to the pole can be distorted by the branch point (threshold) of the complex energy plane where the pole is located. The relevance of the items (i,ii) was demonstrated in Ref. [42].

Clearly, what needs to be done is to replace the BW approximation with the proper pole-extraction method where a unitary coupled-channel amplitude is fitted to the data, and poles on relevant Riemann sheets are searched by analytically continuing the amplitude. This is the main task in this Letter. The pole value not only provides an important knowledge reflecting the QCD dynamics but also serves as a basis for studying the nature of $P_{\psi_s}^\Lambda(4338)$.

Meanwhile, the $M_{J/\psi\Lambda}$ distribution from the LHCb shows a largely fluctuating data point at $M_{J/\psi\Lambda} \sim 4254$ MeV. Seemingly a statistical nature at first glance, the coincidence with the $\Lambda_c\bar{D}_s$ threshold would hint another interesting possibility: a $\Lambda_c\bar{D}_s$ threshold cusp is enhanced by a nearby $P_{\psi_s}^\Lambda(4254)$ pole.

In this work, we conduct a detailed analysis of the LHCb data on $B^- \rightarrow J/\psi\Lambda\bar{p}$. The $M_{J/\psi\Lambda}$, $M_{J/\psi\bar{p}}$, $M_{\Lambda\bar{p}}$, and $\cos\theta_{K^*}$ distribution data are simultaneously fitted with a model in which a unitary $\Xi_c\bar{D}$ - $\Lambda_c\bar{D}_s$ coupled-channel amplitude is implemented. Based on the coupled-channel amplitude, we address the following issues: (i) the $P_{\psi_s}^\Lambda(4338)$ pole position; (ii) a possibility that the $P_{\psi_s}^\Lambda(4338)$ peak is merely a $\Xi_c\bar{D}$ threshold cusp; (iii) implications of the large fluctuation at the $\Lambda_c\bar{D}_s$ threshold.

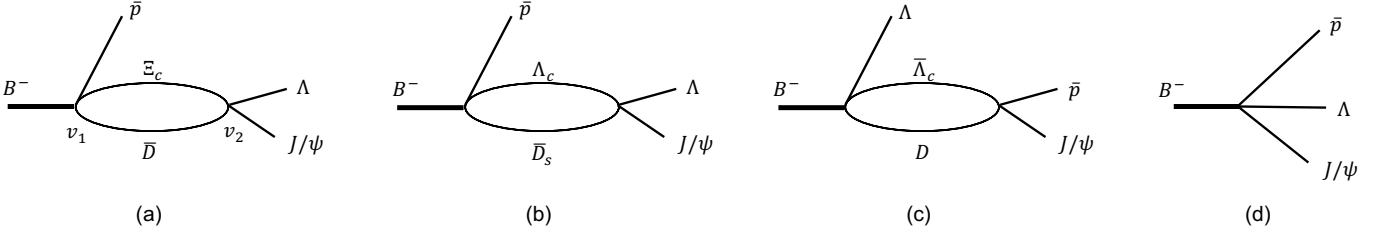


FIG. 1. $B^- \rightarrow J/\psi \Lambda \bar{p}$ mechanisms initiated by weak vertex v_1 of (a) $B^- \rightarrow \Xi_c \bar{D} \bar{p}$; (b) $B^- \rightarrow \Lambda_c \bar{D}_s \bar{p}$; (c) $B^- \rightarrow \bar{\Lambda}_c D \Lambda$; (d) $B^- \rightarrow J/\psi \Lambda \bar{p}$. The second vertex v_2 in (a,b) [(c)] includes a $\Xi_c \bar{D} - \Lambda_c \bar{D}_s$ coupled-channel [$\bar{\Lambda}_c D$ single-channel] scattering, followed by a perturbative transition to $J/\psi \Lambda$ [$J/\psi \bar{p}$].

Model.— The LHCb data shows visible structures only around the $\Xi_c \bar{D}$, $\Lambda_c \bar{D}_s$, and $\bar{\Lambda}_c D$ thresholds. Thus it is reasonable to assume that the structures are caused by the threshold cusps that are further enhanced or suppressed by hadronic rescatterings and the associated poles [43]; see Figs. 1(a-c). Other possible mechanisms are assumed to be absorbed by a direct decay mechanism of Fig. 1(d).

We present amplitude formulas for Figs. 1(a-c). The energy, momentum, and polarization vector of a particle x are denoted by E_x , \mathbf{p}_x , and $\boldsymbol{\epsilon}_x$, respectively, and particle masses are from Ref. [44]. We also denote a baryon(B)-meson(M) pair with J^P by $BM(J^P)$. The initial weak $B^- \rightarrow \Xi_c \bar{D}(1/2^-) \bar{p}$ vertex [Fig. 1(a)] is

$$v_1 = c_{\Xi_c \bar{D} \bar{p}, B^-}^{1/2^-} \langle t_{\bar{D}}^z t_{\bar{D}}^z t_{\Xi_c}^z t_{\Xi_c}^z | 00 \rangle f_{\Xi_c \bar{D}}^0 F_{\bar{p} B^-}^0, \quad (2)$$

with a complex coupling constant $c_{\Xi_c \bar{D} \bar{p}, B^-}^{1/2^-}$. An isospin Clebsch-Gordan coefficient is given by the bracket where $t_x^{(z)}$ is the isospin (z -component) of a particle x . The $B^- \rightarrow \Lambda_c \bar{D}_s(1/2^-) \bar{p}$ [Fig. 1(b)] and $\bar{\Lambda}_c D^0(1/2^+) \Lambda$ [Fig. 1(c)] vertices are the same form with couplings $c_{\Lambda_c \bar{D}_s \bar{p}, B^-}^{1/2^-}$ and $c_{\bar{\Lambda}_c D \Lambda, B^-}^{1/2^+}$. We introduced dipole form factors f_{ij}^L and F_{kl}^L defined by

$$f_{ij}^L = \frac{(1 + q_{ij}^2/\Lambda^2)^{-2 - \frac{L}{2}}}{\sqrt{E_i E_j}}, F_{kl}^L = \frac{(1 + \tilde{p}_k^2/\Lambda^2)^{-2 - \frac{L}{2}}}{\sqrt{E_k E_l}}, \quad (3)$$

where q_{ij} (\tilde{p}_k) is the momentum of i (k) in the ij (total) center-of-mass frame. We use a common cutoff value $\Lambda = 1$ GeV in Eq. (3) for all the interaction vertices. The $B^- \rightarrow \bar{\Lambda}_c D^0 \Lambda$ and $B^- \rightarrow \Lambda_c \bar{D}_s \bar{p}$ decays are color-favored mechanisms, while $B^- \rightarrow \Xi_c \bar{D} \bar{p}$ is color-suppressed.

The above weak decays are followed by hadronic scatterings. We take a data-driven approach to

the hadron interactions while respecting the relevant coupled-channel unitarity; the idea on which the K -matrix approach is also based. We use hadron interactions in a form not biased by any particular models, and all coupling strengths are determined by the data.

We consider the most important coupled-channels: a $\Xi_c \bar{D} - \Lambda_c \bar{D}_s(1/2^-)$ coupled-channel scattering in Figs. 1(a,b), and a $\bar{\Lambda}_c D(1/2^+)$ single-channel scattering in Fig. 1(c). We assume that transitions to the $J/\psi \Lambda$ and $J/\psi \bar{p}$ channels can be treated perturbatively.

We use an s -wave meson-baryon interaction potential:

$$v_{\beta, \alpha}(p', p) = \langle t_{\beta 1} t_{\beta 1}^z t_{\beta 2} t_{\beta 2}^z | 00 \rangle \langle t_{\alpha 1} t_{\alpha 1}^z t_{\alpha 2} t_{\alpha 2}^z | 00 \rangle \times f_{\beta}^0(p') h_{\beta, \alpha} f_{\alpha}^0(p), \quad (4)$$

where α and β label interaction channels such as $\Xi_c \bar{D}(1/2^-)$, and $\alpha 1$ and $\alpha 2$ are the meson and baryon in a channel α , respectively; $h_{\beta, \alpha}$ is a coupling constant. We introduce $[G^{-1}(E)]_{\beta \alpha} = \delta_{\beta \alpha} - h_{\beta, \alpha} \sigma_{\alpha}(E)$ with

$$\sigma_{\alpha}(E) = \sum_{tz} \int dq q^2 \frac{\langle t_{\alpha 1} t_{\alpha 1}^z t_{\alpha 2} t_{\alpha 2}^z | 00 \rangle^2 [f_{\alpha}^0(q)]^2}{E - E_{\alpha 1}(q) - E_{\alpha 2}(q) + i\epsilon}, \quad (5)$$

where \sum_{tz} is needed for $\alpha = \Xi_c \bar{D}$, and $\Xi_c^+ D^-$ and $\Xi_c^0 D^0$ intermediate states with the charge dependent masses are included. The perturbative interactions for $\Xi_c \bar{D}(1/2^-)$, $\Lambda_c \bar{D}_s(1/2^-) \rightarrow J/\psi \Lambda$ and $\bar{\Lambda}_c D^0(1/2^+) \rightarrow J/\psi \bar{p}$ are given by s -wave separable interactions as

$$v_2 = h_{\gamma, \alpha} \langle t_{\alpha 1} t_{\alpha 1}^z t_{\alpha 2} t_{\alpha 2}^z | 00 \rangle \boldsymbol{\sigma} \cdot \boldsymbol{\epsilon}_{\psi} f_{\gamma}^0 f_{\alpha}^0, \quad (6)$$

where $\gamma = J/\psi \Lambda$ or $J/\psi \bar{p}$, and $\boldsymbol{\sigma}$ is the Pauli matrix.

With the above ingredients, the amplitudes for the diagrams of Figs. 1(a,b) and 1(c) are respectively given, following the time-ordered perturbation theory, as

$$A_{\psi \Lambda(1/2^-)}^{1L} = 4\pi \sum_{\alpha, \beta}^{\Xi_c \bar{D}, \Lambda_c \bar{D}_s} h_{\psi \Lambda, \beta} c_{\alpha \bar{p}, B^-}^{1/2^-} \boldsymbol{\sigma} \cdot \boldsymbol{\epsilon}_{\psi} f_{\psi \Lambda}^0(p_{\psi}) \sigma_{\beta}(M_{\psi \Lambda}) G_{\beta \alpha}(M_{\psi \Lambda}) F_{\bar{p} B^-}^0, \quad (7)$$

$$A_{\psi \bar{p}(1/2^-)}^{1L} = 4\pi h_{\psi \bar{p}, \bar{\Lambda}_c D} c_{\bar{\Lambda}_c D \Lambda, B^-}^{1/2^-} \boldsymbol{\sigma} \cdot \boldsymbol{\epsilon}_{\psi} f_{\psi \bar{p}}^0(p_{\psi}) \sigma_{\bar{\Lambda}_c D}(M_{\psi \bar{p}}) G_{\bar{\Lambda}_c D, \bar{\Lambda}_c D}(M_{\psi \bar{p}}) F_{\Lambda B^-}^0. \quad (8)$$

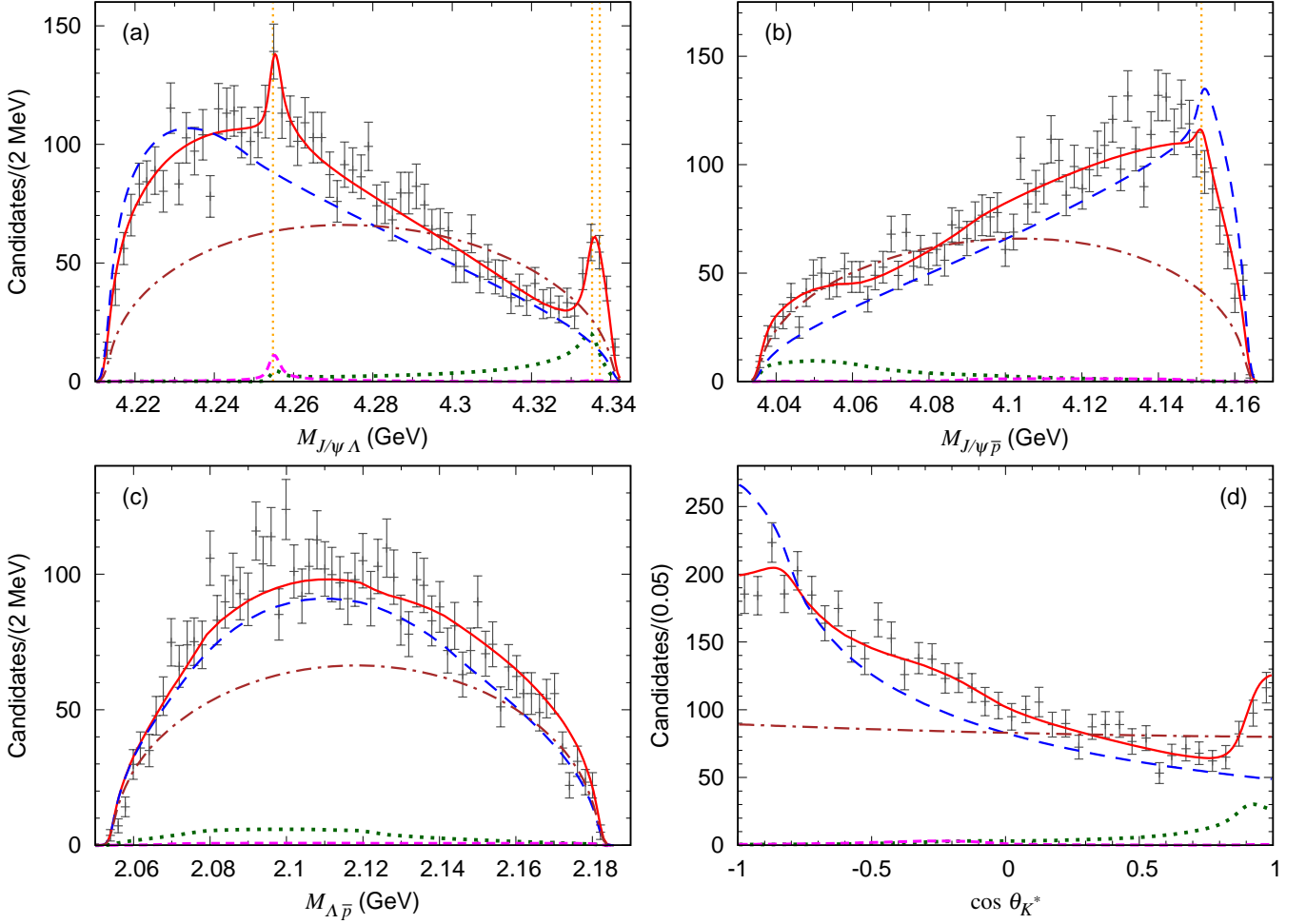


FIG. 2. (a) $J/\psi\Lambda$, (b) $J/\psi\bar{p}$, (c) $\Lambda\bar{p}$ invariant mass distributions and (d) $\cos\theta_{K^*}$ distribution for $B^- \rightarrow J/\psi\Lambda\bar{p}$. The red solid curves are from the default model. Contributions from different initial weak vertices such as $B^- \rightarrow \Xi_c\bar{D}\bar{p}$ [Fig. 1(a), green dotted curve], $B^- \rightarrow \Lambda_c\bar{D}_s\bar{p}$ [Fig. 1(b), magenta short-dashed], $B^- \rightarrow \bar{\Lambda}_c D\Lambda$ [Fig. 1(c), blue long-dashed], and $B^- \rightarrow J/\psi\Lambda\bar{p}$ [Fig. 1(d), brown dash-dotted] are given. All the curves have been smeared with the bin width. The dotted vertical lines indicate thresholds for, from left to right, $\Lambda_c^+ D_s^-$, $\Xi_c^0 \bar{D}^0$, and $\Xi_c^+ D^-$ [$\bar{\Lambda}_c^- D^0$] in the panel (a) [(b)]. Data are from Ref. [36].

The spinors of the final Λ and \bar{p} implicitly sandwich the above expressions.

Regarding the direct decay mechanism of Fig. 1(d), which is color-suppressed, we use the following amplitude for $J/\psi\bar{p}(1/2^+)$ partial wave as

$$A_{\text{dir}} = c_{\text{dir}}^{1/2^+} \boldsymbol{\sigma} \cdot \boldsymbol{\epsilon}_\psi f_{\psi\bar{p}}^0 F_{\Lambda B^-}^0, \quad (9)$$

with a coupling constant $c_{\text{dir}}^{1/2^+}$. We calculate the Dalitz plot distribution using the amplitudes described above, following the procedure detailed in Appendix B of Ref. [45].

Results.— We simultaneously fit the $M_{J/\psi\Lambda}$, $M_{J/\psi\bar{p}}$,

$M_{\Lambda\bar{p}}$, and $\cos\theta_{K^*}$ distributions¹ from the LHCb using the amplitudes of Eqs. (7), (8), and (9). The amplitudes include adjustable coupling constants from the weak vertices of Eq. (2) and from hadronic interactions of Eqs. (4) and (6). We reduce the fitting parameters by setting $h_{\psi\Lambda, \Xi_c\bar{D}} = h_{\psi\Lambda, \Lambda_c\bar{D}_s}$ since the fit quality does not significantly change by allowing $h_{\psi\Lambda, \Xi_c\bar{D}} \neq h_{\psi\Lambda, \Lambda_c\bar{D}_s}$. Then we adjust the products such as $h_{\psi\Lambda, \alpha} c_{\Xi_c\bar{D}\bar{p}, B^-}^{1/2^-}$ in Eqs. (7) and (8). Coupling constants determined by the fit are given in the Supplemental Material. Our default model has 9 fitting parameters in total, considering that the magnitude and phase of the full amplitude are arbitrary.

¹ $\cos\theta_{K^*} \equiv \frac{\mathbf{p}_\Lambda \cdot \mathbf{p}_\psi}{|\mathbf{p}_\Lambda||\mathbf{p}_\psi|}$ in the $\Lambda\bar{p}$ center-of-mass frame.

We show the default model by the red solid curves in Fig. 2, in a good agreement with the LHCb data. In particular, the $P_{\psi_s}^\Lambda(4338)$ and possible $P_{\psi_s}^\Lambda(4254)$ peaks are well fitted. The fit quality is $\chi^2/\text{ndf} = (51 + 96 + 113 + 31)/(235 - 9) \simeq 1.29$ where four χ^2 s are from comparing with the $M_{J/\psi\Lambda}$, $M_{J/\psi\bar{p}}$, $M_{\Lambda\bar{p}}$, and $\cos\theta_{K^*}$ distributions, respectively; 'ndf' is the number of bins (40 for the $\cos\theta_{K^*}$ distribution and 3×65 for the others) subtracted by the number of the fitting parameters.

We also show contributions from the diagrams of Fig. 1 that have different initial weak vertices. Overall, the diagrams of Figs. 1(c) [blue dashed] and 1(d) [brown dash-dotted] dominate the process. The increasing behavior of the spectrum in Fig. 2(b) is understood as the $\bar{\Lambda}_c D$ threshold cusp from Fig. 1(c)². In contrast, the LHCb fitted this behavior with a non-resonant $J/\psi\bar{p}$ [NR($J/\psi\bar{p}$)] amplitude in a polynomial form without identifying the physical origin of the behavior. Still, the coherently summed contribution from Figs. 1(c,d) in our model and the LHCb's NR($J/\psi\bar{p}$) are similar in magnitude. Although the diagrams of Figs. 1(a) [green dotted] and 1(b) [magenta short-dashed] are relatively small in the magnitude, they significantly enhance $\Xi_c \bar{D}$ and $\Lambda_c \bar{D}_s$ threshold cusps, respectively. The LHCb's model generates the $P_{\psi_s}^\Lambda(4338)$ peak with a BW amplitude, and has no other $J/\psi\Lambda$ partial wave amplitude. Thus the partial wave decomposition in the LHCb analysis and ours are fairly similar, although the theoretical descriptions are rather different.

The large contribution from Fig. 1(c) can be understood since it is a color-favored process. The comparable contribution from the color-suppressed Fig. 1(d) may be due to the fact that this mechanism is not suppressed by loops. However, the color-favored contribution from Fig. 1(b) is rather small. This might be because $\Lambda_c \bar{D}_s \rightarrow \Lambda J/\psi$ is suppressed compared with $\bar{\Lambda}_c D \rightarrow \bar{p} J/\psi$. The suppression would be expected since, in a meson-exchange picture, $\Lambda_c \bar{D}_s \rightarrow \Lambda J/\psi$ is caused

TABLE I. $P_{\psi_s}^\Lambda$ poles. (I) default model; (II) [(III)] alternative model with $v_{\Lambda_c \bar{D}_s, \Lambda_c \bar{D}_s} = 0$ [energy dependence of Eq. (10) and $v_{\Lambda_c \bar{D}_s, \Lambda_c \bar{D}_s} = 0$]. Pole positions (in MeV) and their Riemann sheets (see the text for notation) are given in the third and fourth columns, respectively.

(I)	$P_{\psi_s}^\Lambda(4338)$	$(4339.2 \pm 2.7) - (0.9 \pm 0.1) i$	(<i>upp</i>)
	$P_{\psi_s}^\Lambda(4254)$	4254.4 ± 0.8	(<i>upp</i>)
(II)	$P_{\psi_s}^\Lambda(4338)$	$(4336.4 \pm 1.7) + (0.6 \pm 1.5) i$	(<i>ppu</i>)
(III)	$P_{\psi_s}^\Lambda(4338)$	$(4338.4 \pm 4.7) - (7.1 \pm 27.9) i$	(<i>uuu</i>)

² The fit favors a repulsive $\bar{\Lambda}_c D$ interaction, consistent with our previous finding from analyzing $B_s^0 \rightarrow J/\psi p \bar{p}$ [46].

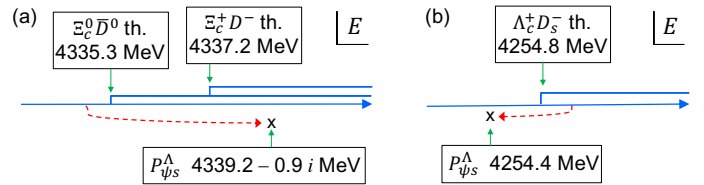


FIG. 3. Pole locations of (a) $P_{\psi_s}^\Lambda(4338)$ and (b) $P_{\psi_s}^\Lambda(4254)$ of the default model. The red dotted arrow indicates how to reach the pole from the closest physical energy region below the $\Xi_c^0 \bar{D}^0$ [above $\Lambda_c^+ \bar{D}_s^-$] threshold in the panel (a) [(b)]. The double lines indicate the branch cuts.

by a $D_s^{(*)}$ -exchange that involves $s\bar{s}$ creation and annihilation while $\bar{\Lambda}_c D \rightarrow \bar{p} J/\psi$ with a $D^{(*)}$ -exchange needs light quark pair (de)excitations. Yet, a solid understanding awaits more detailed theoretical analyses and higher statistics data in the future.

We searched for poles in our default $\Xi_c \bar{D} - \Lambda_c \bar{D}_s(1/2^-)$ coupled-channel scattering amplitude by the analytic continuation. We found $P_{\psi_s}^\Lambda(4338)$ and $P_{\psi_s}^\Lambda(4254)$ poles, as summarized in Table I; J^P is consistent with the LHCb's result for $P_{\psi_s}^\Lambda(4338)$. In the table, we also list the Riemann sheets of the poles by $(s_{\Lambda_c \bar{D}_s}, s_{\Xi_c^0 \bar{D}^0}, s_{\Xi_c^+ D^-})$ where $s_\alpha = p$ or u depending on whether the pole is located on the physical (p) or unphysical (u) sheet of a channel α ³. The pole locations relative to the relevant thresholds are illustrated in Fig. 3. The $P_{\psi_s}^\Lambda(4338)$ pole is mainly generated by $v_{\Xi_c \bar{D}, \Xi_c \bar{D}}$ that is strongly attractive enough to bind them. In fact, if $v_{\Xi_c \bar{D}, \Lambda_c \bar{D}_s}$ is turned off, we still find a pole at 4335.3 MeV which is a bound $\Xi_c^+ D^-$ -virtual $\Xi_c^0 \bar{D}^0$ state. On the other hand, $v_{\Lambda_c \bar{D}_s, \Lambda_c \bar{D}_s}$ is not strong enough to create a $\Lambda_c \bar{D}_s$ bound state but form a virtual pole at 4250.5 MeV. The channel-coupling slightly shifts the pole to the $P_{\psi_s}^\Lambda(4254)$ pole.

Since the light vector-meson exchange between $\Lambda_c \bar{D}_s$ should be suppressed, one may expect $v_{\Lambda_c \bar{D}_s, \Lambda_c \bar{D}_s}$ to be too weak to generate the $P_{\psi_s}^\Lambda(4254)$ pole. A possible explanation for this relatively strong $\Lambda_c \bar{D}_s$ interaction is a two-pion-exchange (TPE) mechanism. TPE mechanisms could be important to understand possible bound states of a bottomonia-pair [47] and a J/ψ - J/ψ pair [48]. Also, a lattice QCD [49] found that a TPE is the dominant long-range part of the ϕ -nucleon interaction, causing a large attraction. In addition, $\Lambda_c \bar{D}_s \rightarrow \Xi_c \bar{D}$ due to a K^* -exchange provides an attraction.

Yet, it is also possible that the fluctuation at the $\Lambda_c \bar{D}_s$ threshold is merely a statistical nature and the $\Lambda_c \bar{D}_s$ interaction is weak. We thus consider an alternative model by removing $v_{\Lambda_c \bar{D}_s, \Lambda_c \bar{D}_s}$ from the default

³ For the definition of (un)physical sheet, see the review section 50 "Resonances" in Ref. [44].

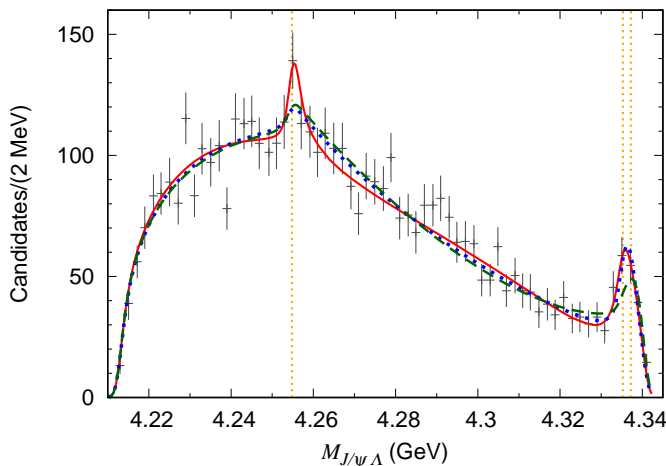


FIG. 4. Comparison of different models. The red solid curve is from the default model while the blue dotted [green dashed] curve is from a model with $v_{\Lambda_c\bar{D}_s, \Lambda_c\bar{D}_s} = 0$ [$v_{\beta, \alpha} = 0$ for all α, β in Eq. (4)]. Other features are the same as Fig. 2(a).

model, refit the data, and show its $M_{J/\psi\Lambda}$ distribution [blue dashed curve] in Fig. 4. The fit quality is $\chi^2/\text{ndf} = (57 + 98 + 106 + 31)/(235 - 8) \simeq 1.29$, similar to the default fit. However, the $\Lambda_c\bar{D}_s$ threshold region is characterized by an ordinary threshold cusp without a nearby pole. The $P_{\psi_s}^\Lambda(4338)$ pole from the alternative model is given in Table I. Interestingly, the default and alternative models have the $P_{\psi_s}^\Lambda(4338)$ poles on different sheets, although their fits are similar in the relevant region. This suggests that the $P_{\psi_s}^\Lambda(4338)$ pole structure may depend on whether a sharp peak exists at the $\Lambda_c\bar{D}_s$ threshold.

We also consider a case where the $\Xi_c\bar{D}$ interaction has an energy-dependence by replacing $h_{\Xi_c\bar{D}, \Xi_c\bar{D}}$ in Eq. (4) with [50]

$$h_{\Xi_c\bar{D}, \Xi_c\bar{D}} + h'_{\Xi_c\bar{D}, \Xi_c\bar{D}} \frac{M_{J/\psi\Lambda}^2 - (m_{\Xi_c} + m_{\bar{D}})^2}{2(m_{\Xi_c} + m_{\bar{D}})}, \quad (10)$$

and $h_{\Lambda_c\bar{D}_s, \Lambda_c\bar{D}_s} = 0$. A comparable fit is obtained: $\chi^2/\text{ndf} = (54 + 95 + 109 + 30)/(235 - 9) \simeq 1.28$. Table I indicates that this model generates a resonance pole for $P_{\psi_s}^\Lambda(4338)$. The width is not well determined probably because the lineshape is largely influenced by the shrinking phase-space and the branch point position. This points to the importance of studying $P_{\psi_s}^\Lambda(4338)$ in $\Xi_b^- \rightarrow J/\psi\Lambda K^-$ where the lineshape reflects the $P_{\psi_s}^\Lambda(4338)$ pole position more directly, thereby discriminating the different $P_{\psi_s}^\Lambda(4338)$ poles in Table I.

We finally examine if the $P_{\psi_s}^\Lambda(4338)$ peak structure is caused merely by the $\Xi_c\bar{D}$ threshold cusp. We fit the data with a non-pole model for which $h_{\beta, \alpha} = 0$ in Eq. (4), and show the result in Fig. 4 by the green dashed curve. While the fit quality, $\chi^2/\text{ndf} = (63 + 105 + 105 +$

$33)/(235 - 5) \simeq 1.33$, is not much worse than the above models overall, the fit in the $P_{\psi_s}^\Lambda(4338)$ peak region is visibly worse. Thus a nearby pole that enhances the cusp is necessary to fit the data.⁴

Summary.— We analyzed the LHCb data on $B^- \rightarrow J/\psi\Lambda\bar{p}$ with a model in Fig. 1; weak B^- decays are followed by coupled-channel scatterings where $P_{\psi_s}^\Lambda$ poles can be developed. Our default model simultaneously fits the $M_{J/\psi\Lambda}$, $M_{J/\psi\bar{p}}$, $M_{\Lambda\bar{p}}$, and $\cos\theta_{K^*}$ distributions; $\chi^2/\text{ndf} \sim 1.29$. We found a $P_{\psi_s}^\Lambda(4338)$ pole at $(4339.2 \pm 2.7) - (0.9 \pm 0.1)i$ MeV. This is the first-time pole determination of the first-discovered hidden-charm pentaquark with strangeness. While the pole determination is important in its own right, it also sets the primary basis for investigating the nature of $P_{\psi_s}^\Lambda(4338)$. The data disfavors the possibility that the $P_{\psi_s}^\Lambda(4338)$ structure is just a kinematical effect. Our default model also fits the fluctuating data point at the $\Lambda_c\bar{D}_s$ threshold, giving a $P_{\psi_s}^\Lambda(4254)$ pole at 4254.4 ± 0.8 MeV. We also considered alternative fits where $P_{\psi_s}^\Lambda(4254)$ does not exist or the $\Xi_c\bar{D}$ interaction has an energy-dependence. We found $P_{\psi_s}^\Lambda(4338)$ poles on different Riemann sheets as summarized in Table I.

This work is in part supported by National Natural Science Foundation of China (NSFC) under contracts U2032103 and 11625523 (S.X.N.) and under Grants No. 12175239 (J.J.W.), and also by National Key Research and Development Program of China under Contracts 2020YFA0406400 (S.X.N., J.J.W.).

Supplemental material

⁴ The same conclusion would follow even considering the triangle-singularity scenario of $P_{\psi_s}^\Lambda(4338)$ [40] since their fit quality in the $P_{\psi_s}^\Lambda(4338)$ region is not better than our non-pole model.

TABLE II. Parameter values for $B^- \rightarrow J/\psi \Lambda \bar{p}$ models. The second, third, and fourth columns are for the default, alternative ($h_{\Lambda_c \bar{D}_s, \Lambda_c \bar{D}_s} = 0$), and no-pole models, respectively. For the arbitrariness, we may multiply a common overall complex factor to the parameters in the 1-4th rows. $h_{\psi \Lambda, \alpha} = h_{\psi \Lambda, \Lambda_c \bar{D}_s} = h_{\psi \Lambda, \Xi_c \bar{D}}$.

$h_{\psi \Lambda, \alpha} c_{\Xi_c \bar{D} \bar{p}, B^-}^{1/2^-}$	$(0.95 \pm 0.28) i$	$(-0.93 \pm 0.33) + (0.83 \pm 0.47) i$	$(2.64 \pm 0.96) + (7.76 \pm 0.39) i$
$h_{\psi \Lambda, \alpha} c_{\Lambda_c \bar{D}_s \bar{p}, B^-}^{1/2^-}$	$(-0.27 \pm 0.08) + (0.25 \pm 0.17) i$	$(-1.25 \pm 0.24) i$	-1.66 ± 0.23
$h_{\psi \bar{p}, \bar{\Lambda}_c D} c_{\bar{\Lambda}_c D \Lambda, B^-}^{1/2^+}$	$(-3.49 \pm 5.27) + (11.82 \pm 3.49) i$	$(-6.32 \pm 4.09) + (10.73 \pm 2.79) i$	$(4.54 \pm 0.38) + (3.49 \pm 1.16) i$
$c_{\text{dir}}^{1/2^+}$	-11.10 ± 2.74	-10.48 ± 2.63	-6.52 ± 1.69
$h_{\Xi_c \bar{D}, \Xi_c \bar{D}}$	-4.97 ± 0.39	-4.00 ± 0.34	0 (fixed)
$h_{\Lambda_c \bar{D}_s, \Lambda_c \bar{D}_s}$	-3.20 ± 0.26	0 (fixed)	0 (fixed)
$h_{\Xi_c \bar{D}, \Lambda_c \bar{D}_s}$	2.76 ± 0.38	-1.68 ± 0.73	0 (fixed)
$h_{\bar{\Lambda}_c D, \bar{\Lambda}_c D}$	3.17 ± 1.83	2.87 ± 1.71	0 (fixed)
Λ (MeV)	1000 (fixed)	1000 (fixed)	1000 (fixed)

TABLE III. Continued from Table II. The second column is for the alternative model with an energy-dependent $\Xi_c \bar{D}$ interaction with the coupling constant $h'_{\Xi_c \bar{D}, \Xi_c \bar{D}}$.

$h_{\psi \Lambda, \alpha} c_{\Xi_c \bar{D} \bar{p}, B^-}^{1/2^-}$	$(3.04 \pm 1.14) + (-2.44 \pm 2.40) i$
$h_{\psi \Lambda, \alpha} c_{\Lambda_c \bar{D}_s \bar{p}, B^-}^{1/2^-}$	$(-0.94 \pm 0.38) i$
$h_{\psi \bar{p}, \bar{\Lambda}_c D} c_{\bar{\Lambda}_c D \Lambda, B^-}^{1/2^+}$	$(-7.50 \pm 5.59) + (9.77 \pm 2.47) i$
$c_{\text{dir}}^{1/2^+}$	-13.15 ± 3.79
$h_{\Xi_c \bar{D}, \Xi_c \bar{D}}$	-2.65 ± 0.85
$h_{\Lambda_c \bar{D}_s, \Lambda_c \bar{D}_s}$	0 (fixed)
$h_{\Xi_c \bar{D}, \Lambda_c \bar{D}_s}$	-2.64 ± 2.07
$h_{\bar{\Lambda}_c D, \bar{\Lambda}_c D}$	2.63 ± 1.89
$h'_{\Xi_c \bar{D}, \Xi_c \bar{D}}$ (MeV $^{-1}$)	-0.34 ± 0.42
Λ (MeV)	1000 (fixed)

- * satoshi@ustc.edu.cn
† wujiajun@ucas.ac.cn
- [1] H.-X. Chen, W. Chen, X. Liu, and S.-L. Zhu, The hidden-charm pentaquark and tetraquark states, *Phys. Rep.* **639**, 1 (2016).
 - [2] A. Hosaka, T. Iijima, K. Miyabayashi, Y. Sakai, and S. Yasui, Exotic hadrons with heavy flavors: X , Y , Z , and related states, *PTEP* **2016**, 062C01 (2016).
 - [3] R.F. Lebed, R.E. Mitchell, and E.S. Swanson, Heavy-Quark QCD Exotica, *Prog. Part. Nucl. Phys.* **93**, 143 (2017).
 - [4] A. Esposito, A. Pilloni, and A.D. Polosa, Multi-quark Resonances, *Phys. Rept.* **668**, 1 (2017).
 - [5] A. Ali, J.S. Lange, and S. Stone, Exotics: Heavy Pentaquarks and Tetraquarks, *Prog. Part. Nucl. Phys.* **97**, 123 (2017).
 - [6] F.-K. Guo, C. Hanhart, U.-G. Meißner, Q. Wang, Q. Zhao, and B.-S. Zou, Hadronic molecules, *Rev. Mod. Phys.* **90**, 015004 (2018).
 - [7] S.L. Olsen, T. Skwarnicki, and D. Zieminska, Nonstandard heavy mesons and baryons: Experimental evidence, *Rev. Mod. Phys.* **90**, 015003 (2018).
 - [8] N. Brambilla, S. Eidelman, C. Hanhart, A. Nefediev, C.-P. Shen, C.E. Thomas, A. Vairo, and C.-Z. Yuan, The XYZ states: Experimental and theoretical status and perspectives, *Phys. Rept.* **873**, 1 (2020).
 - [9] J.-J. Wu, R. Molina, E. Oset and B.-S. Zou, Prediction of narrow N^* and Λ^* resonances with hidden charm above 4 GeV, *Phys. Rev. Lett.* **105**, 232001 (2010).
 - [10] J.-J. Wu, R. Molina, E. Oset and B.-S. Zou, Dynamically generated N^* and Λ^* resonances in the hidden charm sector around 4.3 GeV, *Phys. Rev. C* **84**, 015202 (2011).
 - [11] S.-G. Yuan, K.-W. Wei, J. He, H.-S. Xu and B.-S. Zou, Study of $qqqc\bar{c}$ five quark system with three kinds of quark-quark hyperfine interaction, *Eur. Phys. J. A* **48**, 61 (2012).
 - [12] R. Aaij et al. (LHCb Collaboration), Observation of $J/\psi p$ Resonances Consistent with Pentaquark States in $\Lambda_b^0 \rightarrow J/\psi K^-$ Decays, *Phys. Rev. Lett.* **115**, 072001 (2015).
 - [13] R. Aaij et al. (LHCb Collaboration), Observation of a narrow pentaquark state, $P_c(4312)^+$, and of two-peak structure of the $P_c(4450)^+$, *Phys. Rev. Lett.* **122**, 222001 (2019).
 - [14] C.-W. Xiao, J. Nieves and E. Oset, Prediction of hidden charm strange molecular baryon states with heavy quark spin symmetry, *Phys. Lett. B* **799**, 135051 (2019).
 - [15] H.-X. Chen, L.-S. Geng, W.-H. Liang, E. Oset, E. Wang and J.-J. Xie, Looking for a hidden-charm pentaquark state with strangeness $S = -1$ from Ξ_b^- decay into $J/\psi K^- \Lambda$, *Phys. Rev. C* **93**, 065203 (2016).
 - [16] E. Santopinto and A. Giachino, Compact pentaquark structures, *Phys. Rev. D* **96**, 014014 (2017).
 - [17] C.-W. Shen, J.-J. Wu and B.-S. Zou, Decay behaviors of possible $\Lambda_{c\bar{c}}$ states in hadronic molecule pictures, *Phys. Rev. D* **100**, 056006 (2019).
 - [18] R. Chen, J. He and X. Liu, Possible strange hidden-charm pentaquarks from $\Sigma_c^{(*)}\bar{D}_s^*$ and $\Xi_c^{(*)}\bar{D}^*$ interactions, *Chin. Phys. C* **41**, 103105 (2017).
 - [19] B. Wang, L. Meng and S.-L. Zhu, Spectrum of the strange hidden charm molecular pentaquarks in chiral effective field theory, *Phys. Rev. D* **101**, 034018 (2020).
 - [20] R. Aaij et al. (LHCb Collaboration) Evidence of a $J/\psi\Lambda$ structure and observation of excited Ξ^- states in the $\Xi_b^- \rightarrow J/\psi\Lambda K^-$ decay, *Sci. Bull.* **66**, 1278 (2021).
 - [21] C.-W. Xiao, J.-J. Wu and B.-S. Zou, Molecular nature of $P_{cs}(4459)$ and its heavy quark spin partners, *Phys. Rev. D* **103**, 054016 (2021).
 - [22] F.-Z. Peng, M.-J. Yan, M. Sánchez Sánchez and M.P. Valderrama, The $P_{cs}(4459)$ pentaquark from a combined effective field theory and phenomenological perspective, *Eur. Phys. J. C* **81**, 666 (2021).
 - [23] S. Clymton, H.-J. Kim and H.-C. Kim, Production of hidden-charm strange pentaquarks P_{cs} from the $K^- p \rightarrow J/\psi\Lambda$ reaction, *Phys. Rev. D* **104**, 014023 (2021).
 - [24] Z.-G. Wang and Q. Xin, Analysis of hidden-charm pentaquark molecular states with and without strangeness via the QCD sum rules, *Chin. Phys. C* **45**, 123105 (2021).
 - [25] J.-X. Lu, M.-Z. Liu, R.-X. Shi and L.-S. Geng, Understanding $P_{cs}(4459)$ as a hadronic molecule in the $\Xi_b^- \rightarrow J/\psi\Lambda K^-$ decay, *Phys. Rev. D* **104**, 034022 (2021).
 - [26] M.-W. Li, Z.-W. Liu, Z.-F. Sun and R. Chen, Magnetic moments and transition magnetic moments of P_c and P_{cs} states, *Phys. Rev. D* **104**, 054016 (2021).
 - [27] X. Hu and J. Ping, Investigation of hidden-charm pentaquarks with strangeness $S = -1$, *Eur. Phys. J. C* **82**, 118 (2022).
 - [28] K. Chen, R. Chen, L. Meng, B. Wang and S.-L. Zhu, Systematics of the heavy flavor hadronic molecules, *Eur. Phys. J. C* **82**, 581 (2022).
 - [29] C. Cheng, F. Yang and Y. Huang, Searching for strange hidden-charm pentaquark state $P_{cs}(4459)$ in $\gamma p \rightarrow K^+ P_{cs}(4459)$ reaction, *Phys. Rev. D* **104**, 116007 (2021).
 - [30] H.-X. Chen, W. Chen, X. Liu and X.-H. Liu, Establishing the first hidden-charm pentaquark with strangeness, *Eur. Phys. J. C* **81**, 409 (2021).
 - [31] Z.-G. Wang, Analysis of the $P_{cs}(4459)$ as the hidden-charm pentaquark state with QCD sum rules, *Int. J. Mod. Phys. A* **36**, 2150071 (2021).
 - [32] K. Azizi, Y. Sarac and H. Sundu, Investigation of $P_{cs}(4459)^0$ pentaquark via its strong decay to $\Lambda J/\psi$, *Phys. Rev. D* **103**, 094033 (2021).
 - [33] R. Chen, Can the newly $P_{cs}(4459)$ be a strange hidden-charm $\Xi_c\bar{D}^*$ molecular pentaquarks?, *Phys. Rev. D* **103**, 054007 (2021).
 - [34] M.-Z. Liu, Y.-W. Pan and L.-S. Geng, Can discovery of hidden charm strange pentaquark states help determine the spins of $P_c(4440)$ and $P_c(4457)$?, *Phys. Rev. D* **103**, 034003 (2021).
 - [35] W.-Y. Liu, W. Hao, G.-Y. Wang, Y.-Y. Wang, E. Wang and D.-M. Li, The resonances $X(4140)$, $X(4160)$, and $P_{cs}(4459)$ in the decay of $\Lambda_b \rightarrow J/\psi\Lambda\phi$, *Phys. Rev. D* **103**, 034019 (2021).
 - [36] Chen Chen and Elisabetta Spadaro on behalf of the LHCb Collaboration, New tetra- and pentaquarks at LHCb, LHC Seminar, <https://indico.cern.ch/event/1176505/>.
 - [37] M. Karliner and J. R. Rosner, New strange pentaquarks, arXiv:2207.07581.
 - [38] F.-L. Wang and X. Liu, Emergence of molecular-type characteristic spectrum of hidden-charm pentaquark with strangeness embodied in the $P_{\psi_s}^\Lambda(4338)$ and $P_{cs}(4459)$, arXiv:2207.10493.
 - [39] M.-J. Yan, F.-Z. Peng, M. S. Sánchez, and M.P. Valderrama, The $P_{\psi_s}^\Lambda(4338)$ pentaquark and its partners in the molecular picture, arXiv:2207.11144.

- [40] T.J. Burns and E.S. Swanson, The LHCb state $P_{\psi_s}^\Lambda(4338)$ as a triangle singularity, arXiv:2208.05106.
- [41] F.-K. Guo, X.-H. Liu, and S. Sakai, Threshold cusps and triangle singularities in hadronic reactions, Prog. Part. Nucl. Phys. **112**, 103757 (2020).
- [42] L. Meng, B. Wang, and S.-L. Zhu, The double thresholds distort the lineshapes of the $P_{\psi_s}^\Lambda(4338)^0$ resonance, arXiv:2208.03883.
- [43] X.-K. Dong, F.-K. Guo, and B.-S. Zou, Explaining the Many Threshold Structures in the Heavy-Quark Hadron Spectrum, Phys. Rev. Lett. **126**, 152001 (2021).
- [44] P.A. Zyla et al. (Particle Data Group), The Review of Particle Physics, Prog. Theor. Exp. Phys. **2020**, 083C01 (2020).
- [45] H. Kamano, S.X. Nakamura, T.-S.H. Lee, and T. Sato, Unitary coupled-channels model for three-mesons decays of heavy mesons, Phys. Rev. D **84**, 114019 (2011).
- [46] S.X. Nakamura, A. Hosaka, and Y. Yamaguchi, $P_c(4312)^+$ and $P_c(4337)^+$ as interfering $\Sigma_c \bar{D}$ and $\Lambda_c \bar{D}^*$ threshold cusps, Phys. Rev. D **104**, L091503 (2021).
- [47] N. Brambilla, G. Krein, J.T. Castellà, and A. Vairo, Long-range properties of $1S$ bottomonium states, Phys. Rev. D **93**, 054002 (2016).
- [48] X.-K. Dong, V. Baru, F.-K. Guo, C. Hanhart, A. Nefediev, and B.-S. Zou, Is the existence of a $J/\psi J/\psi$ bound state plausible? Sci. Bull. **66**, 2462 (2021).
- [49] Y. Lyu, T. Doi, T. Hatsuda, Y. Ikeda, J. Meng, K. Sasaki, and T. Sugiura, Attractive N - ϕ Interaction and Two-Pion Tail from Lattice QCD near Physical Point, arXiv:2205.10544 [hep-lat].
- [50] M.-L. Du, M. Albaladejo, F.-K. Guo, and J. Nieves, Combined analysis of the $Z_c(3900)$ and the $Z_{cs}(3985)$ exotic states, Phys. Rev. D **105**, 074018 (2022).